Thermal Diffuse Scattering of Low-Energy Electrons from Xe†

L. L. Kesmodel and F. W. de Wette
Department of Physics, University of Texas, Austin, Texas 78712
and
R. E. Allen
Department of Physics, Texas A & M University, College Station, Texas 77843

(Received 1 May 1972)

One-phonon thermal-diffuse-scattering intensities have been calculated for the (111), (100), and (110) surfaces of Xe. The calculations are based on the (pseudo-) kinematical approximation, which is presumably very good for this material. The finite penetration of the electrons into the crystal is approximately taken into account with a transmission factor. As we have pointed out previously, it is important to include the penetration since the assumption of scattering from the surface layer only (made in treatments by other authors) leads to results which are qualitatively incorrect. The present calculations are for extensive regions of reciprocal space including several reciprocal lattice rods. The results are presented in the form of both contour curves and intensity profiles. Several interesting features are apparent, including (i) anisotropies about the reciprocal lattice rods, (ii) differences in intensity distributions around different rods which are caused by interference effects (and which therefore provide a measure of the attenuation of the electron beam), and (iii) the presence of an "extra spot" in the results for the (100) surface. It is possible that these qualitative features can be observed in low-energy electron diffraction experiments on other monatomic fcc materials.

I. INTRODUCTION

Recently, Ignatiev, Rhodin, and co-workers have succeeded in performing low-energy electron-diffraction (LEED) measurements on Xe films.[1,2] These measurements provide an excellent opportunity for comparisons between theory and experiment, because (a) the interaction between Xe atoms can be approximated by the simple Lennard–Jones potential and (b) it appears that low-energy electron scattering from Xe, unlike that from most other materials, can be treated successfully with the simple kinematical approximation.[1,2] In view of these recent experiments, we have considered it worthwhile to perform extensive calculations of the one-phonon kinematical thermal diffuse scattering (TDS) from Xe. Our calculations are for the (111), (100), and (110) surfaces, with the (111) orientation being of the greatest immediate interest because it occurs in the films studied in Refs. 1 and 2.

A second motivation for the present work is the possibility that, within the kinematical approximation, the qualitative results may be applicable to other monatomic fcc materials.

II. GENERAL FORMULATION

As is well known, the Bragg peaks associated with scattering from the bulk of a crystal undergo a decrease in intensity as the temperature is increased. The intensity which is lost from the Bragg peaks goes into TDS. Whereas the Bragg scattering is concentrated only at reciprocal lattice points, the TDS is distributed throughout all of reciprocal space. In the case of scattering from a surface, the Bragg scattering is concentrated at "reciprocal lattice rods" associated with the two-dimensional reciprocal lattice points for the surface, and the TDS is again distributed throughout reciprocal space.

In the present work, we will treat the TDS within the framework of the (pseudo-) kinematical approximation; i.e., we will adopt the picture that an electron undergoes only one scattering process within the solid, and we will include the effect of attenuation of the electron beam through a transmission factor. There is evidence that this approximation provides a good description of low-energy electron diffraction from Xe for beam energies above 40 eV.[1,2] It is also worth mentioning that a calculation by Moon[3] for the TDS from Cu, which included dynamical (multiple scattering) effects, gave approximately the same values for the intensities as a kinematical calculation.

In our calculations we will consider only the one-phonon contribution to the thermal diffuse scattering, as described below. At high temperatures multiphonon processes become increasingly important. For Xe and other sufficiently heavy materials, however, the one-phonon scattering should dominate at low enough temperatures. We will also make the quasiharmonic approximation, which is known to be valid for Xe (as well as Ar and Kr) at sufficiently low temperatures.[4]

For convenience, our calculations are performed for a slab-shaped crystal nine layers in thickness. The results for such a model should approximate the results for a semi-infinite crystal except for a small region near each reciprocal lattice rod (see Sec. III). The last important approximation

involved in our calculations is the assumption of a Lennard–Jones 12-6 potential to describe the interaction between Xe atoms. This potential yields rather accurate results for a number of bulk properties of the noble-gas solids.[4]

As usual,[5] we take the z direction to be perpendicular to the surface, and we adopt periodic boundary conditions in the x-y plane. We restrict the discussion to monatomic crystals for which we can specify each particle by a two-dimensional lattice point $\bar{l}=(l_1, l_2)$ and an index l_3 which specifies a layer parallel to the surface. We will use the convention of writing the planar part of a vector with bars; e.g., $\vec{r}=(x, y, z)=\bar{r}+z\hat{z}$, where $\hat{z}$ is the unit vector normal to the surface. The instantaneous position of an atom within the crystal is given by

$$\vec{r}(\bar{l}, l_3)=\vec{r}_0(\bar{l}, l_3)+\vec{u}(\bar{l}, l_3)\ , \tag{2.1}$$

where $\vec{r}_0(\bar{l}, l_3)$ is the mean position of the atom and $\vec{u}(\bar{l}, l_3)$ is the time-dependent displacement.

Within the kinematical and quasiharmonic approximations, the one-phonon thermal-diffuse-scattering intensity $I_1(\vec{Q})$ is given by[6]

$$I_1(\vec{Q})=I_0|f_0|^2\sum_{\bar{l},\bar{l}',l_3,l_3'}\alpha(l_3)\alpha(l_3')\,e^{-M(\bar{l},l_3)}e^{-M(\bar{l}',l_3')}\times\exp\{i\vec{Q}\cdot[\vec{r}_0(\bar{l}, l_3)-\vec{r}_0(\bar{l}', l_3')]\}\times\langle[\vec{Q}\cdot\vec{u}(\bar{l}, l_3)][\vec{Q}\cdot\vec{u}(\bar{l}', l_3')]\rangle\ , \tag{2.2}$$

where I_0 is the incident intensity, f_0 is the atomic scattering factor, $\alpha(l_3)$ is the transmission factor for the plane labeled by l_3, $\vec{Q}$ is the difference between the wave vectors of the scattered and incident waves, and the angular brackets indicate a thermal average. The quantity $e^{-M(\bar{l},l_3)}$ is the square root of the Debye–Waller factor, i.e.,

$$M(\bar{l}, l_3)=\tfrac{1}{2}\langle[\vec{Q}\cdot\vec{u}(\bar{l}, l_3)]^2\rangle\ . \tag{2.3}$$

For crystal surfaces having the symmetries of those that we will consider, one can show that $\langle u_\alpha u_\beta\rangle=0$ if $\alpha\neq\beta$ $(\alpha=x, y, z)$ so that

$$M(\bar{l}, l_3)=M(l_3)=\tfrac{1}{2}\sum_\alpha Q_\alpha^2\langle u_\alpha^2(l_3)\rangle\ . \tag{2.4}$$

The mean-square amplitudes $\langle u_\alpha^2(l_3)\rangle$ have been previously calculated[5] from the equation

$$\langle u_\alpha^2(l_3)\rangle=\frac{\hbar}{2\bar{N}M}\sum_{\bar{k},p}\frac{|\xi_\alpha(l_3;\bar{k}p)|^2}{\omega_p(\bar{k})}\coth\left(\frac{\hbar\omega_p(\bar{k})}{2k_BT}\right)\ , \tag{2.5}$$

where $\bar{N}$ is the number of values of the wave vector $\bar{k}$ occurring in the summation, M is the atomic mass, p distinguishes the vibrational frequencies $\omega_p(\bar{k})$ for a given $\bar{k}$, $\xi_\alpha(l_3;\bar{k}p)$ is an eigenvector which specifies the direction of vibration for a given vibrational mode, k_B is the Boltzmann constant, and T is the temperature. In the summation of Eq. (2.5) and in the following, the phonon wave vector $\bar{k}$ is to be restricted to the first (two-dimensional) Brillouin zone associated with the surface.

Equation (2.2) can be cast into a more usable form by writing $\vec{u}(\bar{l}, l_3)$ in terms of the normal coordinates[7] $A(\bar{k}p)$:

$$\vec{u}(\bar{l}, l_3)=(\bar{N}M)^{-1/2}\sum_{\bar{k},p}A(\bar{k}p)\vec{\xi}(l_3;\bar{k}p)\,e^{i\bar{k}\cdot\bar{r}_0(\bar{l},l_3)}\ . \tag{2.6}$$

If one substitutes Eq. (2.6) into Eq. (2.2) and uses the result for the ensemble average of the normal coordinates[8]

$$\langle A(\bar{k}p)A^*(\bar{k}'p')\rangle=\Delta(\bar{k}-\bar{k}')\delta_{pp'}\frac{\hbar}{2\omega_p(\bar{k})}\coth\left(\frac{\hbar\omega_p(\bar{k})}{2k_BT}\right) \tag{2.7}$$

[with $\Delta(\bar{k}-\bar{k}')=1$ if $(\bar{k}-\bar{k}')$ is a planar reciprocal lattice vector $\bar{G}$ and $\Delta(\bar{k}-\bar{k}')=0$ otherwise], then the scattering intensity can be expressed in terms of the normal mode frequencies and eigenvectors:

$$I_1(\vec{Q})=I_0|f_0|^2\frac{\hbar\bar{N}}{2M}\sum_{l_3,l_3'}\alpha(l_3)\alpha(l_3')e^{-M(l_3)}e^{-M(l_3')}\times\exp\{iQ_z[z_0(l_3)-z_0(l_3')]\}\sum_p[\vec{Q}\cdot\vec{\xi}(l_3;\bar{Q}p)^*]\times[\vec{Q}\cdot\vec{\xi}(l_3';\bar{Q}p)]\frac{1}{\omega_p(\bar{Q})}\coth\left(\frac{\hbar\omega_p(\bar{Q})}{2k_BT}\right)\ . \tag{2.8}$$

Once the frequencies and eigenvectors have been determined as in Ref. 5, it is in principle straightforward to calculate the TDS intensity for a given value of $\vec{Q}$.[9] In the remainder of this paper we discuss such calculations for the noble-gas solids. Two preliminary reports of these calculations have been given previously.[10,11]

III. PROCEDURE OF CALCULATIONS

We assume a Lennard-Jones potential of interaction between the noble-gas atoms,

$$\phi(r)=4\epsilon[(\sigma/r)^{12}-(\sigma/r)^6]\ , \tag{3.1}$$

with the potential parameters ϵ and σ having the values given by Horton.[12] We define the dimensionless temperature

$$T^*=(k_B/\hbar)(M\sigma^2/\epsilon)^{1/2}T \tag{3.2}$$

and the dimensionless frequency

$$\omega^*=(M\sigma^2/\epsilon)^{1/2}\omega\ , \tag{3.3}$$

so that Eq. (2.8) becomes

$$I_1(\vec{Q})=I_0|f_0|^2\frac{\hbar\bar{N}}{2a^2}\left(\frac{\sigma^2}{M\epsilon}\right)^{1/2}I^*(\vec{Q})\ , \tag{3.4}$$

where $a\sqrt{2}$ is the nearest-neighbor distance and the dimensionless quantity $I^*(\vec{Q})$ is given by

$$I^*(\vec{Q})=a^2\sum_{l_3,l_3'}\alpha(l_3)\alpha(l_3')\,e^{-M(l_3)}e^{-M(l_3')}$$

$$\times \exp\{iQ_z[z_0(l_3) - z_0(l_3')]\} \sum_p [\vec{\mathbf{Q}} \cdot \vec{\xi}(l_3; \overline{\mathbf{Q}}p)^*]$$

$$\times [\vec{\mathbf{Q}} \cdot \vec{\xi}(l_3'; \overline{\mathbf{Q}}p)] \frac{1}{\omega_p^*(\overline{\mathbf{Q}})} \coth\left(\frac{\omega_p^*(\overline{\mathbf{Q}})}{2T^*}\right) . \quad (3.5)$$

In the present calculations the eigensystem was determined for nine-layer slabs having (111), (110), and (100) surface orientations. The static relaxation of the planes near the surface and the resulting change in force constants were taken into account.[5] The transmission factor $\alpha(l_3)$ was taken to decrease geometrically with increasing distance into the crystal from the surface, with the ratio $\alpha(l_3 - 1)/\alpha(l_3) = 0.5$ unless otherwise stated. The top five layers ($l_3 = 1, \ldots, 5$, with $l_3 = 5$ at the surface) were included in the calculation of I^* from Eq. (3.5). It is important to note that the transmission factor $\alpha(l_3)$ is a phenomenological parameter incorporated in a kinematical description of the scattering to account for attenuation as the beam penetrates the crystal. Since $\alpha(l_3)$ is a function of the electron energy and the angle of incidence, our choice of $\alpha(l_3)$ will be valid only for particular scattering conditions. However, we have carried out test calculations for other choices of $\alpha(l_3)$ (see below), and we find that the main results are not strongly sensitive to the value of the ratio $\alpha(l_3 - 1)/\alpha(l_3)$.

In order to directly relate I^* to an observed scattering intensity, it is necessary to eliminate effects due to the factor $|f_0|^2$, since f_0 depends on the scattering angle. This is accomplished by holding the magnitude of the scattering vector, $|\vec{\mathbf{Q}}|$, fixed while the planar vector $\overline{\mathbf{Q}}$ is varied. In an actual scattering experiment this procedure corresponds to tilting and rotating the crystal while keeping the rest of the apparatus, and thus the scattering angle, fixed.[13] The results for I^* are, therefore, presented as a function of $\overline{\mathbf{Q}}$ in a two-dimensional reciprocal space appropriate for the given surface and for constant $|\vec{\mathbf{Q}}|$. The results cover extensive regions of reciprocal space including a number of reciprocal lattice rods.

It should be noted here, as discussed in an earlier paper,[10] that the slab-model calculation does not give physically realistic results for the scattering intensity at very small values of $|\overline{\mathbf{Q}} - \overline{\mathbf{G}}|$ — that is, for points very near the reciprocal lattice rods. The reason for this failing of the slab model is that the finite thickness of the slab results in a finite sum over the index p in Eq. (2.8). In the slab model with N_3 planes, there are $3N_3$ modes in this summation, whereas in a semi-infinite crystal there are an infinite number of modes. For all values of $\overline{\mathbf{Q}}$ except those very near the reciprocal lattice rods, the frequencies of the modes are rather evenly spaced and the finite slab model gives an accurate sampling of the modes in a semi-infinite crystal. However, in the immediate vicinity of the reciprocal lattice rods $\overline{\mathbf{G}}$, there are three modes whose frequencies $\omega(\overline{\mathbf{Q}})$ go to zero as $|\overline{\mathbf{Q}} - \overline{\mathbf{G}}|$ goes to zero and which consequently dominate the summation over p in Eq. (2.8); since the sample modes are no longer evenly spaced, the results for the semi-infinite crystal and the crystal of finite thickness will be considerably different. For example, in the high-temperature limit one can easily show that $I_1(\vec{\mathbf{Q}})$ goes as $|\overline{\mathbf{Q}} - \overline{\mathbf{G}}|^{-2}$ as $|\overline{\mathbf{Q}} - \overline{\mathbf{G}}| \to 0$ in the model of a slab with finite thickness. However, Wallis and Maradudin[14] and Huber[15] have shown that for a semi-infinite crystal, in the continuum approximation and the high-temperature limit, $I_1(\vec{\mathbf{Q}})$ goes as $|\overline{\mathbf{Q}} - \overline{\mathbf{G}}|^{-1}$ as $|\overline{\mathbf{Q}} - \overline{\mathbf{G}}| \to 0$, and McKinney, Jones, and Webb[13] have experimentally verified this result. The method we have described, then, is not valid for calculating the scattering intensity for a semi-infinite crystal in the immediate vicinity of a reciprocal lattice rod. However, a conservative estimate based on earlier high-temperature results for the slab model[10] indicates that the model is invalid in regions around reciprocal lattice rods having areas of only a few percent of the first Brillouin zone. We consequently regard the finite slab model as quite useful for studies of the scattering intensity in large regions of reciprocal space.

IV. RESULTS AND DISCUSSION

In this section we present the results for the thermal diffuse scattering from the (111), (100), and (110) surfaces of xenon using the method outlined above. In all cases the temperature T is 23.3 °K ($T^* = 10.0$) and for each surface the magnitude of the scattering vector $|\vec{\mathbf{Q}}| = (Q_x^2 + Q_y^2 + Q_z^2)^{1/2}$ is fixed at a particular value. The intensity I^* is

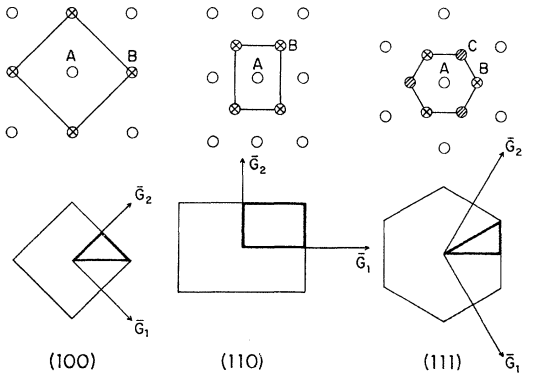

FIG. 1. Surface unit cells and Brillouin zones for the (100), (110), and (111) surfaces of a monatomic fcc crystal. The stacking is *ABAB* ... for the (100) and (110) surfaces and *ABCABC*... for the (111) surface.

given as a function of $\vec{Q} = (Q_x, Q_y)$ in the surface reciprocal lattice space appropriate to each surface. In Fig. 1 we show the orientation of the two-dimensional unit cell and Brillouin zone for each surface. The positions of the atoms of each layer and the stacking order are also indicated. The primitive-surface reciprocal lattice vectors $\vec{G}_1$ and $\vec{G}_2$ are shown and are used in defining the reciprocal lattice rods (mn) corresponding to $\vec{G} = m\vec{G}_1 + n\vec{G}_2$.

In Figs. 2–4 results are shown for the (111) surface with $|\vec{Q}| = 6\pi\sqrt{3}/a$ corresponding to a (666) reflection—that is, for the sixth diffraction maximum along the (00) rod arising from the resid-

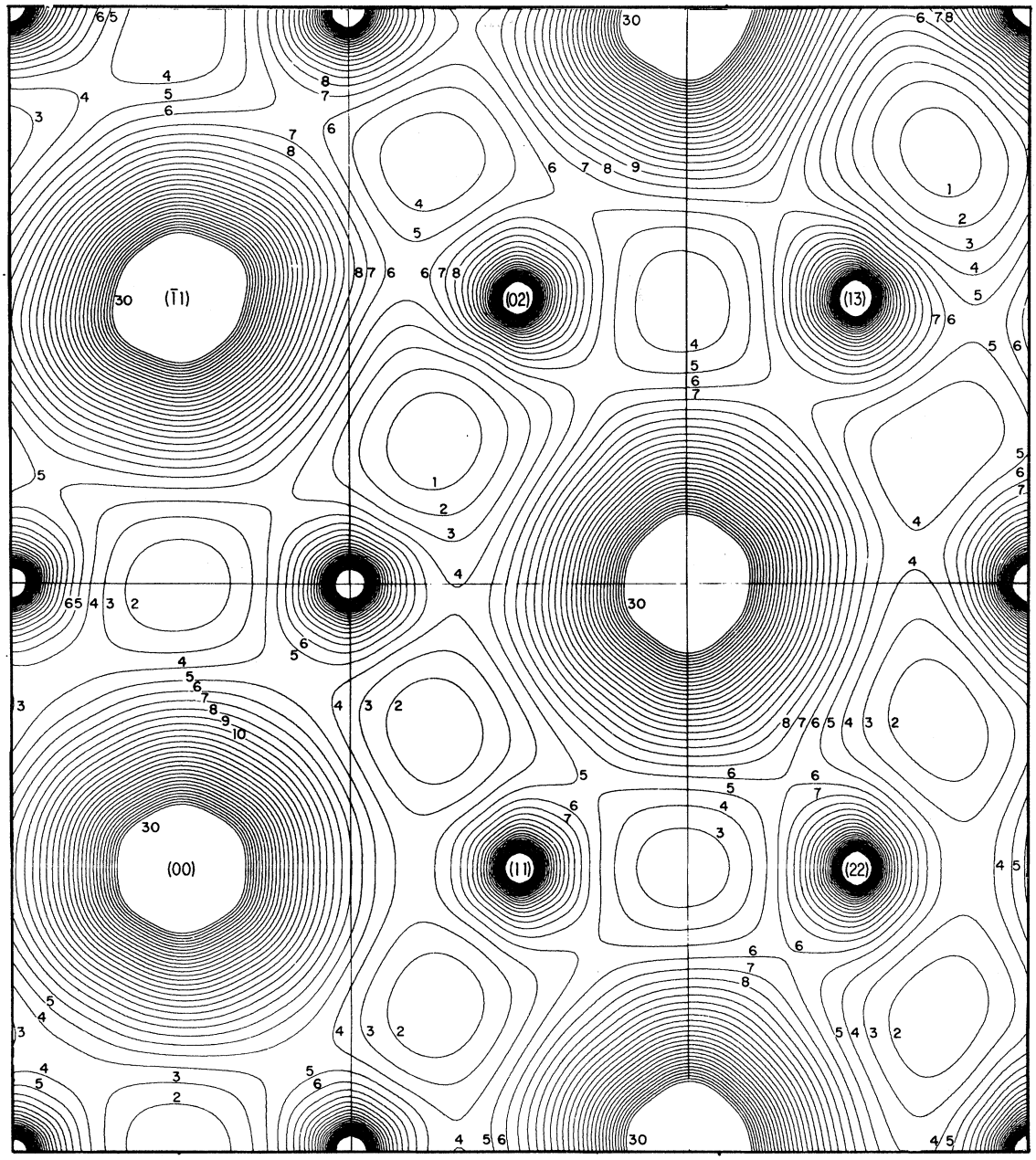

FIG. 2. Curves of equal intensity for (111) surface of Xe, at a temperature of 23.3 °K and for $|\vec{Q}| = 6\pi\sqrt{3}/a$, where $a\sqrt{2}$ is the nearest-neighbor distance. The value of I^* along the curve labeled n is given by $\log_{10} I^* = (0.02379) \times (n-1) + 1.31000$. Curves for which $n > 30$, e.g., near the (00) rod, are not shown. The curves were determined by interpolation between points on an 80×80 grid in each of the rectangular areas centered on a reciprocal lattice rod.

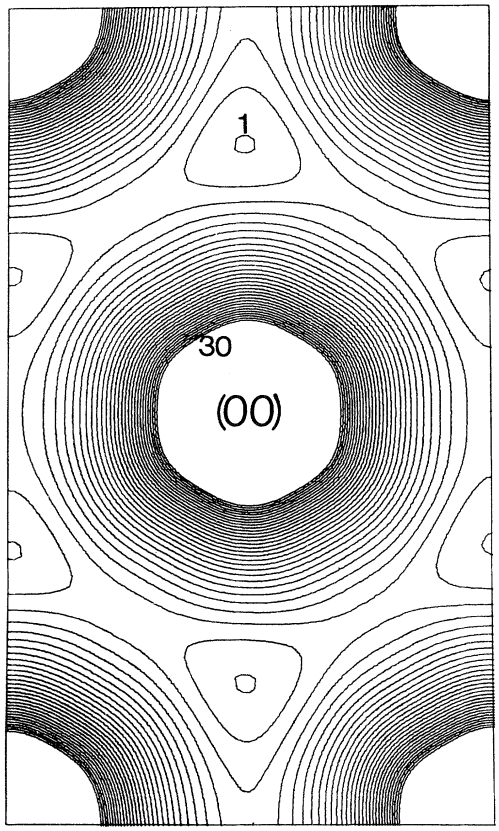

FIG. 3. Monolayer scattering from Xe (111) to be compared with the region around the (00) rod of Fig. 2. The plot is on a logarithmic scale as in Fig. 2 with values indexed from 1 to 30, but quantitative values are not given.

ual third Laue equation. Figure 2 shows the curves of equal intensity, which are logarithmically spaced. Representative reciprocal lattice rods (mn) are so labeled, e.g., (00) and (11). One finds that the pattern indeed has a point symmetry similar to that of the slab. For example, there is an exact threefold symmetry about the (00) rod, but only an approximate sixfold symmetry. The intensities are peaked as expected around reciprocal lattice rods. However, there are considerable differences in intensities around different rods. These differences can be largely understood in terms of interference between layers arising from the finite penetration of the electrons. That is, the two-dimensional periodicity of the lattice gives rise to the maxima at the rods, but the effects of penetration will modify these maxima differently at different rods. The differences in the intensity distributions around different rods thus gives an indication of how rapidly the electron beam is attenuated with distance into the crystal. In order to illustrate this effect of the penetration, we have performed a monolayer calculation (scattering from the surface only), the results of which are shown in Fig. 3; these results are to be compared with the region around the (00) rod in Fig. 2. Recall that in the multilayer scattering we have included five layers and have used $\alpha(l_3-1)/\alpha(l_3)=0.5$. One notes the large qualitative differences between multilayer and monolayer scattering. In Fig. 4 a profile of I^* vs $\bar{Q}$ is shown for values of $\bar{Q}$ lying between the (00) rod and the point $(\frac{5}{2}\,\frac{5}{2})$.

Similar results for the (100) and (110) surfaces are shown in Figs. 5–10 with $|\vec{Q}| = 12\pi/a$ [(600) reflection] and $12\pi\sqrt{2}/a$ [(660) reflection], respectively. As in the case of the (111) surface, the patterns reflect the symmetry of the slabs and exhibit strong interference features not present in monolayer calculations. An additional feature in the (100) results is the presence of an "extra spot" near the (04) rod appearing in Figs. 5 and 7. This local maximum arises from constructive interference between the planes of atoms parallel to the surface. That is, at the position of the occurrence of the extra spot the scattering vector $\vec{Q}$ is passing through a region in reciprocal space characterized by constructive interference between the planes.

In the above discussion we have alluded to the importance of interference between layers in connection with the structure of the TDS around the reciprocal lattice rods and also in connection with the extra spot in the (100) results. A principal

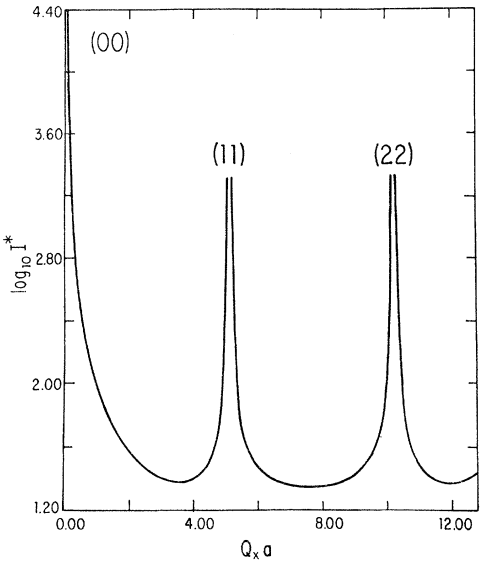

FIG. 4. I^* vs $\bar{Q}$ for values of $\bar{Q}$ lying between the points (00) and $(\frac{5}{2}\,\frac{5}{2})$ for Xe (111) at $T=23.3$ °K and $|\vec{Q}| = 6\pi\sqrt{3}/a$.

conclusion from these results is that the main features of the TDS can be understood in terms of the familiar Ewald diagram. Namely, there are large peaks in the intensity when the scattering vector crosses a reciprocal lattice rod, and the relative strengths of these peaks depends on the distance along the rod to a Laue maximum. Moreover, small peaks (extra spots) can arise in the TDS intensity away from the rods when the scattering vector passes through a region satisfying the residual third Laue equation (i.e., as determined by Q_z). However, the quantitative importance of these effects will, of course, be determined by the attenuation of the electron beam with distance into the crystal. The extreme case of scattering from the surface layer only was discussed above and illustrated in Figs. 3, 6, and 9. In this case there is no interference between layers and we thus find similar behavior near all the rods. In order to further demonstrate the effects of interference, we show in Fig. 11 graphs of I^* vs $|\vec{Q}|$ for the (100) surfac for three additional values of the ratio $\alpha(l_3-1)/\alpha(l_3)$—namely, 0.6, 0.4, and 0.2. These values are representa-

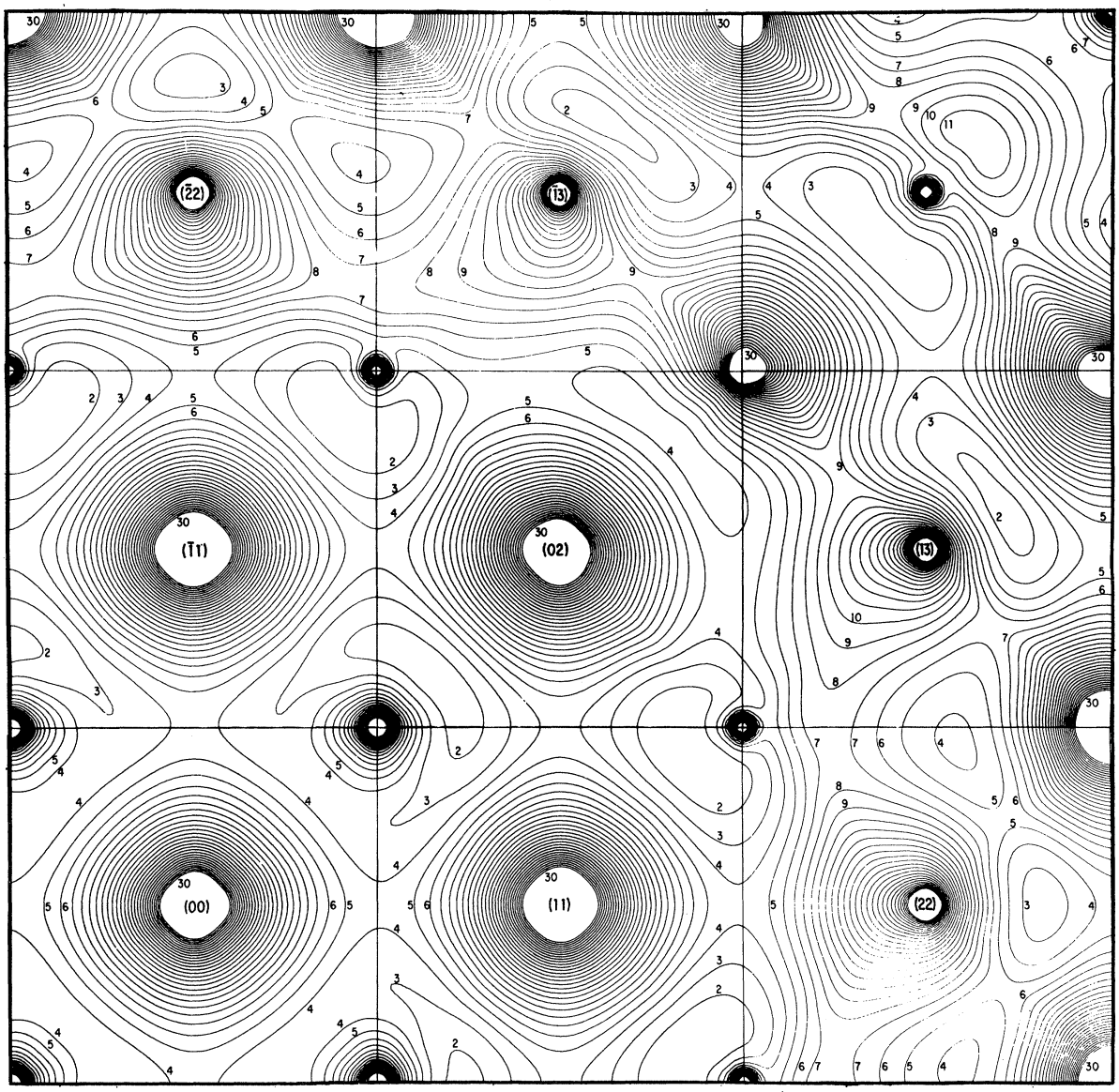

FIG. 5. Curves of equal intensity for (100) surface of Xe, at a temperature of 23.3 °K and for $|\vec{Q}| = 12\pi/a$. The value of I^* along the curve labeled n is given by $\log_{10} I^* = (0.03241) \times (n-1) + 1.06000$.

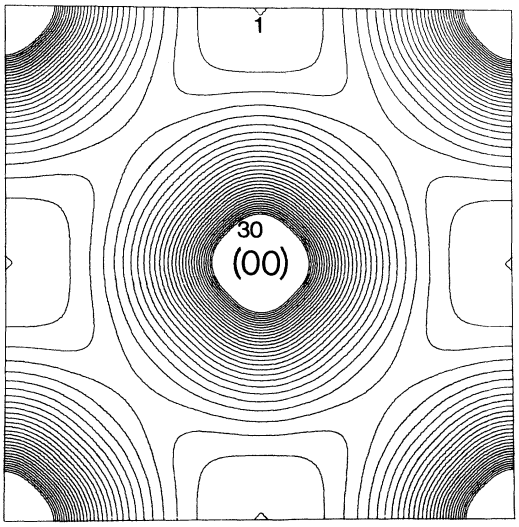

FIG. 6. Monolayer scattering from Xe (100) to be compared with the region around the (00) rod of Fig. 5.

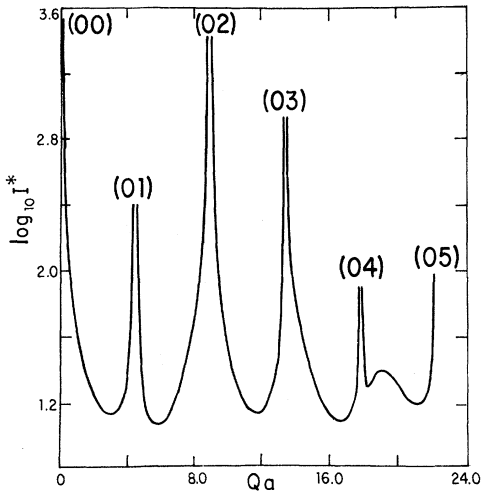

FIG. 7. I^* vs $Q = |\vec{Q}| = (Q_x^2 + Q_y^2)^{1/2}$ for values of $\vec{Q}$ lying between the (00) and (05) rods for Xe (100) at $T = 23.3$ °K and $|\vec{Q}| = 12\pi/a$. Note the "extra spot" just beyond the (04) rod.

tive of the attenuation for energies relevant to LEED.[16] It can be seen that the extra spot is more prominent for a ratio of 0.6 and less prominent at 0.4 than it is in the results of Fig. 7 for a ratio of 0.5, and that it is absent in the results for 0.2. These results demonstrate that the extra spot is

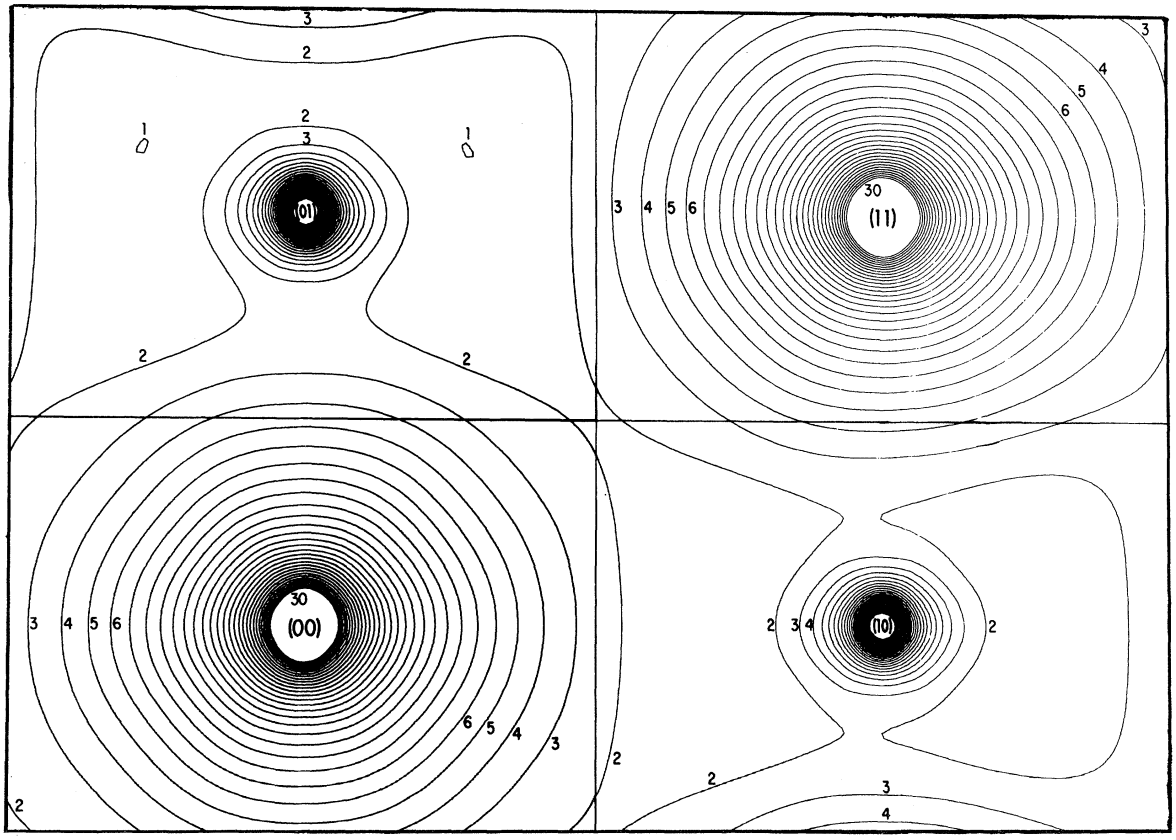

FIG. 8. Curves of equal intensity for (110) surface of Xe, at a temperature of 23.3 °K and for $|\vec{Q}| = 12\pi\sqrt{2}/a$. The value of I^* along the curve labeled n is given by $\log_{10} I^* = (0.05525) \times (n-1) + 0.09770$.

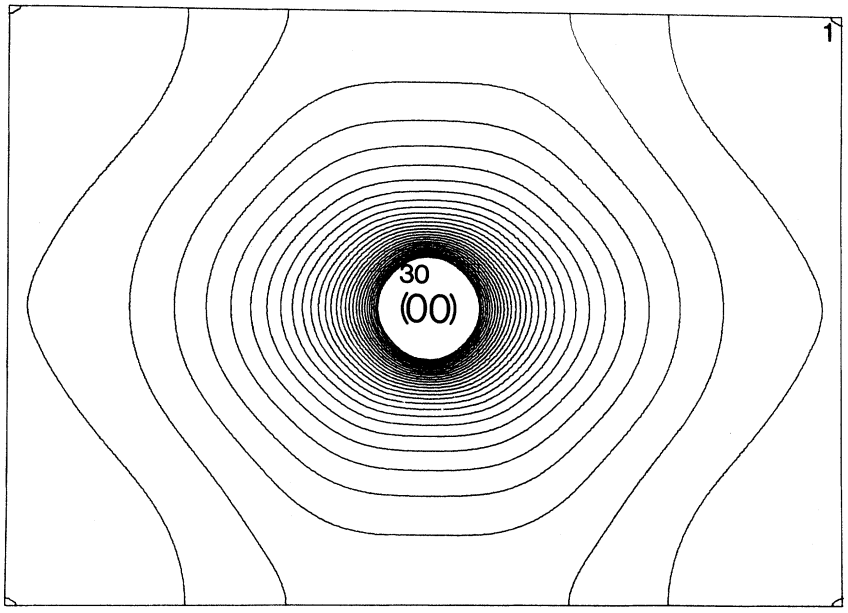

FIG. 9. Monolayer scattering from Xe (110) to be compared with the region around the (00) rod of Fig. 8.

due to interplanar interference; i.e., as the attenuation increases and the effective interference between planes consequently decreases, the extra spot is diminished. The relative heights of the peaks at the rods shown in Fig. 11 also behave with attenuation in the way discussed above, the peaks becoming more equal as the attenuation is increased. It is worthwhile to note, however, that the relative heights are not strongly sensitive to the value of the ratio $\alpha(l_3-1)/\alpha(l_3)$, and the range 0.2–0.6 probably corresponds to a rather wide range in beam energy.[16]

In conclusion, these calculations illustrate the important qualitative properties of the TDS in the framework of the pseudokinematical theory. It is clear that there are strong interplanar interference effects that modify the scattering along

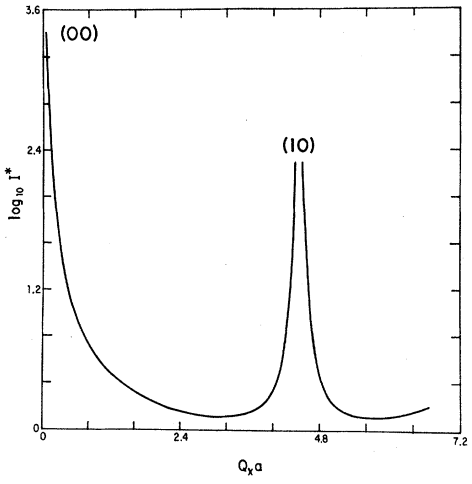

FIG. 10. I^* vs $\bar{Q}$ for values of $\bar{Q}$ lying between the (00) and $(\frac{3}{2}\ 0)$ points for Xe (110) at $T=23.3$ °K and $|\bar{Q}| = 12\pi\sqrt{2}/a$.

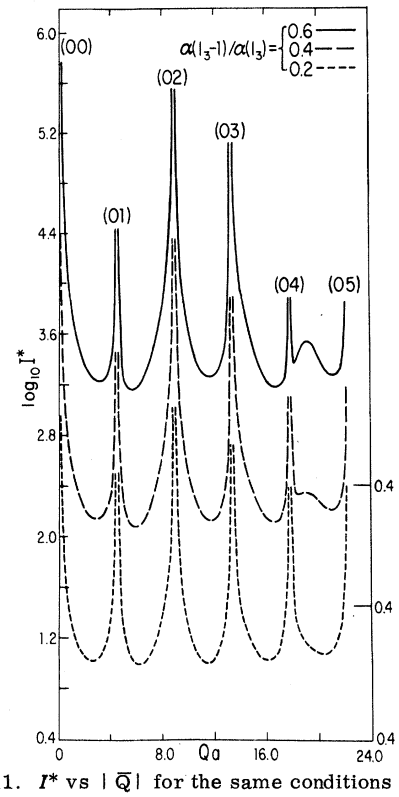

FIG. 11. I^* vs $|\bar{Q}|$ for the same conditions as in Fig. 7 but for three values of the ratio $\alpha(l_3-1)/\alpha(l_3)$: 0.2 (rapid attenuation), 0.4, 0.6 [in Fig. 7, $\alpha(l_3-1)/\alpha(l_3)=0.5$]. The graphs for 0.4 and 0.6 are shifted upwards as indicated at the right-hand side of the figure.

the rods. As discussed above, these interference features provide a measure of the attenuation of the electron beam with distance into the crystal. The combined effects of interference and the vibrational properties of the atoms gives rise to considerable detail in the predicted intensity patterns. It would be of interest to see how these predictions compare with experiments on xenon and other monatomic fcc materials.

ACKNOWLEDGMENT

One of the authors (L. L. K) wishes to thank Dr. G. P. Alldredge for many helpful discussions in the course of this work.

†Research sponsored by the U. S. Air Force Office of Scientific Research (AFSC) under Grant No. 71-1973.

[1]A. Ignatiev, J. B. Pendry, and T. N. Rhodin, Phys. Rev. Lett. **26,** 189 (1971).

[2]A. Ignatiev, T. N. Rhodin, S. Y. Tong, B. I. Lundqvist, and J. B. Pendry, Solid State Commun. **9,** 1851 (1971).

[3]A. R. Moon, Z. Naturforsch. A **25,** 752 (1970).

[4]See, e.g., M. L. Klein, G. K. Horton, and J. L. Feldman, Phys. Rev. **184,** 968 (1969); F. W. de Wette and R. M. J. Cotterill, Solid State Commun. **6,** 227 (1968); F. W. de Wette, L. H. Fowler, and B. R. A. Nijboer, Physica (Utr.) **54,** 292 (1971).

[5]R. E. Allen and F. W. de Wette, Phys. Rev. **179,** 873 (1969).

[6]A. A. Maradudin, E. W. Montroll, G. H. Weiss, and I. P. Ipatova, *Theory of Lattice Dynamics in the Harmonic Approximation,* 2nd ed. (Academic, New York, 1971), p. 597.

[7]R. E. Allen, G. P. Alldredge, and F. W. de Wette, Phys. Rev. B **4,** 1648 (1971).

[8]See Ref. 6, p. 60.

[9]We mention one point which requires some care: According to the convention we use in defining the dynamical matrix (see Ref. 7), the eigenvectors $\xi_\alpha(l_3;\bar{k}p)$ are changed by a phase factor if a reciprocal lattice vector $\bar{G}$ is added to $\bar{k}$. In the calculations of Ref. 10, it was assumed in the case of the (100) surface that $\xi_\alpha(l_3;\bar{k}p)$ was invariant under the translation $\bar{k}\rightarrow\bar{k}+\bar{G}$; consequently the results for the (100) surface in Ref. 10 are in error. This error was, of course, corrected in the calculations of the present paper.

[10]F. W. de Wette and R. E. Allen, in *The Structure and Chemistry of Solid Surfaces*, edited by G. A. Somorjai (Wiley, New York, 1969).

[11]L. L. Kesmodel, F. W. de Wette, and R. E. Allen, Solid State Commun. **11,** 145 (1972).

[12]G. K. Horton, Am. J. Phys. **36,** 93 (1968).

[13]J. T. McKinney, E. R. Jones, and M. B. Webb, Phys. Rev. **160,** 523 (1967).

[14]R. F. Wallis and A. A. Maradudin, Phys. Rev. **148,** 962 (1966).

[15]D. L. Huber, Phys. Rev. **153,** 772 (1967).

[16]E. R. Jones, J. T. McKinney, and M. B. Webb, Phys. Rev. **151,** 476 (1966).

PHYSICAL REVIEW B VOLUME 7, NUMBER 2 15 JANUARY 1973

Reorientation and Motion of the Self-Trapped Hole in $KMgF_3$†

J. T. Lewis,* J. L. Kolopus,‡ E. Sonder, and M. M. Abraham
Solid State Division, Oak Ridge National Laboratory, Oak Ridge, Tennessee 37830
(Received 24 July 1972)

The thermal motion of the self-trapped hole in $KMgF_3$ has been investigated by observing the decay of $[F_2^-]$-center aligment as a function of time and temperature. Electron-paramagnetic-resonance [EPR] and polarized-optical-absorption techniques were used. The results show that reorientation through an angle of $\pi/2$ takes place in the range 90–100 K with an activation energy of 0.260 eV. Reorientation through an angle of $\pi/3$ takes place, but at a temperature about 10 K higher, and with an activation energy of 0.29 eV. Annealing of the self-trapped holes occurs between 100 and 110 K. The kinetics are not simple first or second order, but are what would be expected if the self-trapped holes could either annihilate with their complementary electrons or be retrapped at other trapping sites. Consideration of all possible ways in which holes can migrate or reorient suggests that the annealing occurs via a linear motion along [110] rows of F^- ions and does not involve any reorientation of the $[F_2^-]$ centers.

I. INTRODUCTION

Self-trapped holes have been observed in numerous halide crystals.[1] They are of particular interest since they exhibit many characteristics normally associated with ionic defects or impurities (e.g., paramagnetic resonance and optical absorption) yet do not involve any missing or excess ions in the lattice. They have been studied in greatest detail in alkali-halide crystals, for which the details of the optical and EPR spectra as well as the details of hole motion are well understood. At low temperatures, if an electron is ionized from one of the halide ions and is trapped elsewhere, the resulting halide atom shares the hole with a neighboring ion, forming an $[X_2^-]$ molecular ion, the interionic spacing of which is significantly smaller than the nearest-neighbor spacing of the halide ions in the perfect lattice.[2] It is this relaxation that permits the self-trapping of the hole. As the temperature is raised, the self-trapped hole moves by hopping. In materials having the NaCl struc-